Acta Materialia 122 (2017) 266–276

Contents lists available at ScienceDirect

Acta Materialia

journal homepage: www.elsevier.com/locate/actamat

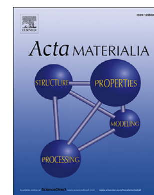

Full length article

Compositionally graded ferroelectrics as wide band gap semiconductors: Electrical domain structures and the origin of low dielectric loss

I.B. Misirlioglu [a,*], S.P. Alpay [b,c]

[a] Faculty of Engineering and Natural Sciences, Sabanci University, Tuzla, Orhanli, 34956 Istanbul, Turkey
[b] Department of Materials Science and Engineering and Institute of Materials Science, University of Connecticut, Storrs, CT 06269, USA
[c] Department of Physics, University of Connecticut, Storrs, CT 06269, USA

ARTICLE INFO

Article history:
Received 27 May 2016
Received in revised form
22 September 2016
Accepted 27 September 2016

Keywords:
Graded thin films
Ferroelectric
Dielectric constant
Semiconductor
Thermodynamics

ABSTRACT

Functional materials with compositional gradients exhibit unique characteristics that are different from the components comprising the structure. Graded ferroelectrics are very good examples to such materials where a systematic variation in composition is introduced along the thickness of a thin film heterostructure. Such structures display interesting properties including the disappearance of the dielectric anomaly at the ferroelectric-paraelectric transition that is otherwise observed in monolayer ferroelectrics, a strong internal ("built-in") electric field, low dielectric loss, and an almost temperature insensitive dielectric tunability. We present here a theoretical study to understand some interesting properties of graded ferroelectrics by treating these as wide band gap semiconductors. Such an approach allows us to address the effect of impurities/dopants. We specifically analyze compositionally graded (001) heteroepitaxial (Pb,Sr)TiO_3 films between Pt electrodes on (001) $SrTiO_3$. Our analysis shows that a single-domain state could be stabilized in the presence of space charges whereas intrinsic stacks display wedge-like electrical domain patterns. The computations also provide an explanation as to why graded ferroelectrics should have lower dielectric losses and lower leakage currents compared to monolayer ferroelectrics. We attribute this to the carrier depletion in the layers due to built-in electric fields resulting from the polarization mismatch.

© 2016 Acta Materialia Inc. Published by Elsevier Ltd. All rights reserved.

1. Introduction

Designing materials that are specifically engineered to exhibit particular properties or fulfill a specific functionality has become a routine practice due to developments in modern synthesis and fabrication methods. Introducing compositional gradients has proven to be an effective method, for instance, in impeding crack propagation in structural components, enabled by elastic interactions between layers of different composition [1,2]. This has led to significant improvements in areas such as the aerospace propulsion industry where functionally graded materials are employed as thermal barrier coatings in turbine blades to extend their lifetime [3]. In analogy, electrostatic interactions between ferroelectric layers with differing Curie temperatures (T_C) can be employed to adjust properties of these systems and may even allow additional functionalities not found in any of the compositions comprising the structure [4–17]. Such an approach has already been employed in generating what one calls "piezoelectric doping" in wide bandgap polar GaN/AlN superlattices where the polarization jumps between layers of different stoichiometry is further enhanced upon varying the external stress on the system or choice of the substrate, altering the "sheet" carrier densities at the layer interfaces [18–21]. Compositional variations in ferroelectrics (FEs) also generate strong internal long-range (volumetric) electric fields which are responsible for unique hysteresis response and dielectric, piezoelectric, and pyroelectric properties [4,6,7,10,12,15–17,22–27]. Such interactions, however, in a compositionally graded ferroelectric (gFE) can be quite complex as the system minimizes the total free energy via making adjustments to polarization in the presence of coupled tensorial property coefficients of various ranks. That the ferroelectric polarization in a given coordinate inside the material can reversibly adjust itself both by means of orientation and amplitude to any type of boundary condition (elastic or electrostatic) is making the case rather complicated, rendering intuitive

* Corresponding author.
E-mail address: burc@sabanciuniv.edu (I.B. Misirlioglu).

http://dx.doi.org/10.1016/j.actamat.2016.09.050
1359-6454/© 2016 Acta Materialia Inc. Published by Elsevier Ltd. All rights reserved.

guesses about these systems quite difficult as we shall show. Moreover, since FEs are wide band gap semiconductors [28,29], the electrical boundary conditions at the surfaces and interfaces are expected to play a significant role in the ultimate electrical and dielectric properties of such materials. For example, it is important whether a film is grown on a substrate or is a free-standing construct, what kind of electrodes are used, what the "strength" of grading is, not to mention the magnitude of the strain gradients that result from polarization variations and possible strain relaxation mechanisms [4,5,8,9,11,12,22–24,30–47].

In gFEs, the highly non-linear nature of the electrostatic and electromechanical interactions between layers makes it extremely difficult to establish a direct link between observed properties and polarization variations. This is compounded by the fact that interlayer interactions depend on the electrical boundary conditions, electrode material, the misfit strain between layers as well as the layers and the substrate if in thin film form, and defect microstructures that include stacking faults, ferroelastic twins, misfit and threading dislocations, and a host of point defects like ionizable impurities including oxygen or other vacancies. Such complexities have resulted in several theoretical and computational studies to understand and to describe dielectric, piezoelectric, and pyroelectric properties often determined by sophisticated measurements and precise materials characterization methods where the sensitivity of ferroics to microstructure need to be considered exclusively [48–51]. Experimental studies reported relative (small-signal) dielectric permittivities ranging from several hundred to several thousand in high quality compositionally graded $BaTiO_3$ with altered Ba-site stoichiometry along the thickness in a wide range of temperatures (T) [8,52,53]. What is also interesting is that there is no anomaly in the temperature dependence of the dielectric response within the temperature span that was chosen in this study which is in the spectra of bulk Curie temperatures, T_C, of the constituent layers. It is known that internal (depolarizing) electric fields resulting from polarization mismatches will always reduce the polarization in the layer with the highest T_C which tend to suppress the global transition temperature of the entire stack. This reduction is accompanied by a strong smearing of the paraelectric (PE) – FE phase transition of the entire heterostructure, giving rise to a high dielectric response that is temperature insensitive over a relatively broad temperature range. Similar results have also been observed in monolithic FE films with "dead" layers at the electrode/FE interfaces, different (asymmetric) top/bottom electrodes, and FE superlattices consisting of periodic units [54–56], but compositionally gFEs display unique characteristics (such as very high dielectric response even far below the global T_C, low loss and dependence of electrical properties on the sequence of the grading with respect to the gFE/substrate interface) that require a more realistic treatment or interpretation that must employ a thorough electrostatic analysis.

A notable characteristic of graded ferroelectrics is the low loss dielectric response especially at low frequencies. For typical dielectrics, the ratio of the imaginary part of the dielectric function to the real part ($\tan\cdot\delta$) decreases with increasing frequencies as $\tan\cdot\delta$ (which is a function of the electrical conductivity) is inversely proportional to applied signal frequency. A comparison of experimental results in monolayer (Ba,Sr)TiO_3 films and graded (Ba,Sr) TiO_3 systems shows that there is almost an order of magnitude difference in $\tan\cdot\delta$ in the low signal frequency regimes where conduction losses are expected to dominate [8,52,53]. There has been some discussion on the nature of this rather unexpected property that is observed in both epitaxial and polycrystalline multilayers [57]. However, the origin of this important phenomenon is not clear. Low dielectric loss is one of the counterintuitive properties of gFE systems we would like to describe, at least qualitatively, in this study. A careful understanding of this occurrence would have tremendous implications in terms of the development of next generation of capacitors, piezoelectric sensors and actuators, and pyroelectric energy conversion devices.

Here, we develop a theoretical approach based on principles of non-linear thermodynamics which is coupled with a detailed electrostatic analysis taking into account that FEs are in fact wide band gap semiconductors [28] as these materials possess band gaps around 3 eV [29]. Our goal is to shed light on the electrical domain structures, polarization stabilities, phase transformations characteristics and dielectric properties of mesoscopic compositionally gFEs. We first develop a theoretical framework for metal/gFE/metal heterostructures and then apply this approach to (001) heteroepitaxial graded $Pb_xSr_{1\text{-}x}TiO_3$ (gPST) between Pt electrodes on (001) $SrTiO_3$ (ST) substrates (Pt/gPST/Pt). We specifically analyze gPST numerically in the absence and presence of charged defects, in particular n-type impurities defined through the Fermi-Dirac distribution considering the gPST as a wide band gap polar semiconductor. We show that the dielectric anomaly in intrinsic stacks disappears in contrast to what is observed in monolayer films and this is related to the strong smearing of the FE phase transition as well as the electrical domain structures. Presence of relatively small concentrations of ionizable impurities (that often form unintentionally during processing of such structures such as oxygen or A-site vacancies in ABO_3 perovskite FEs) of the order of 10^{25} m^{-3}[58] can have an impact on the domain stabilities and dielectric response of the structures, owing to the complex electrostatic interaction between the charges introduced by the impurities and the polarization gradients, an outcome that has almost never been discussed for gPSTs. We also observe that intrinsic stacks (in the same sense as the semiconductor terminology) are entirely in a multi-domain (MD) state where the domain structure transitions from a typical rectangular stripe domain pattern in the high T_C layer towards a more diffuse "sinusoidal" morphology in the low T_C layer. Band bending and charge distributions inside the graded heterostructures we compute allow us to explain qualitatively the low loss behavior of gPSTs.

2. Theory and methodology

The schematic of the gPST heterostructures analyzed here and the strength of the compositional gradient introduced are provided in Fig. 1. We define this strength as the range of the ferroelectric transition temperatures (T_C) of layers that make up the construct. We consider two stacks labeled as "coarse" gPST and "smooth" gPST. The very top layer in our analysis is $PbTiO_3$ (PT) and for coarsely gPST the compositional variation is introduced by replacing 10% of Pb in PT by Sr at every 12.5 nm. For smooth gPST stacks, 5% of Pb is replaced with Sr at every 6.75 nm. The total thickness of both heterostructures is 100 nm. The material parameters of each layer are assumed to be a weighted linear average of the constituents, namely PT and ST in the following manner:

$$s^f = (1-f)\cdot s^{PT} + f\cdot s^{ST} \quad (1)$$

where s^f is any material parameter, such as the band gap, thermodynamic stiffness coefficients, unit cell lattice parameter, of a layer corresponding to a particular fraction, f, of Sr replacing Pb ions in the lattice, s^{PT} and s^{ST} are any given material parameter for pure PT and ST, respectively. f varies in this model from 0 to 0.7, corresponding to a range of Curie temperatures from that of pure PT in bulk (~765 K) all the way to ~200 K for $f = 0.7$. Averaging of material properties, both thermodynamic, structural and electronic, is an approximation to serve as a means to provide us with the results that can be used to interpret certain electrical behavior observed in

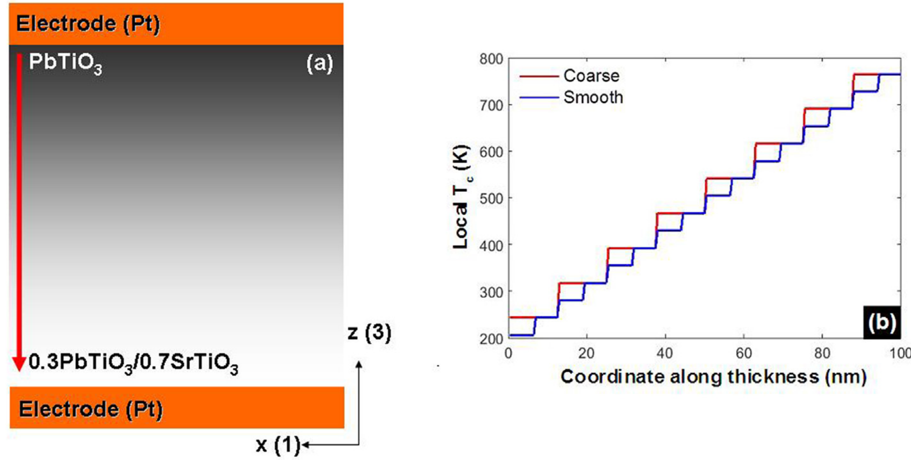

Fig. 1. Schematic representation of **(a)** the graded PST heterostructure analyzed in this study and **(b)** the local bulk T_C going from PT to PST with $f = 0.7$ as a function of the position along the *z*-axis. In (b), the grading schemes employed in the computations are also identified. For coarsely and smoothly gPST, the compositional variation is introduced by replacing 10% of Pb in PT by Sr at every 12.5 nm and 5% of Pb replaced with Sr at every 6.75 nm, respectively.

these structures. We also note that in such a system that we have computationally designed, the overall PE-FE phase transformation temperature $<T_C>$ will depend on the elastic and electrostatic BCs. This will be discussed in the subsequent sections.

The total energy density of such a compositionally gFE heterostructure is essentially the sum of the free energies of each layer that are coupled to each other electrostatically and electromechanically, i.e.:

$$F_S = \sum_f \left[\int_V F_{FE}^f dV \right] \tag{2}$$

where the integration is over the volumetric free energies of each individual layer and F_{FE}^f is the Landau-Ginzburg-Devonshire (LGD) energy of a layer given by:

$$\begin{aligned} F_{FE}^f = {} & \alpha_1\left(P_1^2+P_2^2+P_3^2\right)+\alpha_{11}\left(P_1^4+P_2^4+P_3^4\right)+\alpha_{12}\left(P_1^2P_2^2\right. \\ & \left.+P_1^2P_3^2+P_2^2P_3^2\right)+\alpha_{111}\left(P_1^6+P_2^6+P_3^6\right)+\alpha_{112}\left[P_1^4\left(P_2^2\right.\right. \\ & \left.\left.+P_3^2\right)+P_2^4\left(P_1^2+P_3^2\right)+P_3^4\left(P_1^2+P_2^2\right)\right]+\alpha_{123}P_x^2P_y^2P_z^2 \\ & -\frac{1}{2}S_{11}\left(\sigma_1^2+\sigma_2^2+\sigma_3^2\right)-S_{12}(\sigma_1\sigma_2+\sigma_1\sigma_3+\sigma_2\sigma_3) \\ & -\frac{1}{2}S_{44}\left(\sigma_4^2+\sigma_5^2+\sigma_6^2\right)-Q_{11}\left(\sigma_1P_1^2+\sigma_2P_2^2+\sigma_3P_3^2\right) \\ & -Q_{12}\left[\sigma_1\left(P_2^2+P_3^2\right)+\sigma_2\left(P_1^2+P_3^2\right)+\sigma_3\left(P_1^2+P_2^2\right)\right]+F_G^f \end{aligned} \tag{3}$$

where

$$\begin{aligned} F_G^f = {} & G_{33}\left(\frac{dP_3}{dz}\right)^2+G_{31}\left(\frac{dP_3}{dx}\right)^2+G_{13}\left(\frac{dP_1}{dz}\right)^2+G_{11}\left(\frac{dP_1}{dx}\right)^2 \\ & +G_{23}\left(\frac{dP_2}{dz}\right)^2+G_{21}\left(\frac{dP_2}{dx}\right)^2+G_{32}\left(\frac{dP_3}{dy}\right)^2+G_{22}\left(\frac{dP_2}{dy}\right)^2 \\ & +G_{12}\left(\frac{dP_1}{dy}\right)^2 \end{aligned} \tag{4}$$

for each layer. In Eqs (3) and (4), P_i ($i = 1,2,3$) is the polarization vector, σ_i ($i = 1,2,\ldots,6$) is the (applied) stress tensor in contracted (Voigt) notation, S_{ij} and Q_{ij} are the elastic compliances (again in Voigt notation) at constant polarization and electrostrictive coefficients, respectively, α_i, α_{ij}, and α_{ijk} are dielectric stiffness (Landau) coefficients, and G_{ij} are gradient energy coefficients. For each layer *f*, these parameters are determined from Eq. (1).

Taking into account that the top surface of the entire stack is traction free results in some simplification since σ_3, σ_4, σ_5, and σ_6 vanish, leaving us only with the in plane misfit stresses σ_1 and σ_2 that can be expressed in terms of the in-plane (polarization-free) misfit strain u_m for each layer such that $\sigma_1 = \sigma_2 = C_{11}\mu_m + C_{12}(u_m + u_3)$ where u_3 is the stress-free out-of-plane strain and C_{ij} are elastic constants at constant polarization. We point out that u_m varies with layer composition in accordance with lattice parameters obtained via Eq. (1), which we denote as u_m^f. We assume that the gradient energy coefficients are isotropic and approximately the same for all compositions not to complicate further the analysis. In addition, variations in gradient energy due to possible anisotropy of this coefficient are negligibly small compared to electrostatic energy for the range of thicknesses considered in this work and by no means change the physics of the problem. Eq. (3) can be written in terms of elastic compliances and in any given layer, $dF_{FE}^f/d\sigma_i = u_m^f$ ($i = 1, 2$) to express the in-plane stresses σ_1 and σ_2 in terms of u_m^f and P_i reducing Eq. (3) to:

$$\begin{aligned} F_{FE}^f = {} & \alpha_1^{fm}\left(P_1^2+P_2^2\right)+\alpha_3^{fm}P_3^2+\alpha_{11}^{fm}\left(P_1^4+P_2^4\right)+\alpha_{33}^{fm}P_3^4 \\ & +\alpha_{13}^{fm}\left(P_1^2P_3^2+P_2^2P_3^2\right)+\alpha_{12}^{fm}P_1^2P_2^2+\alpha_{111}\left(P_1^6+P_2^6+P_3^6\right) \\ & +\alpha_{112}\left[P_1^4\left(P_2^2+P_3^2\right)+P_2^4\left(P_1^2+P_3^2\right)+P_3^4\left(P_1^2+P_2^2\right)\right] \\ & +\alpha_{123}P_1^2P_2^2P_3^2+u_m^2\big/(S_{11}+S_{12})+G\left[\left(\frac{dP_3}{dz}\right)^2+\left(\frac{dP_3}{dx}\right)^2\right. \\ & \left.+\left(\frac{dP_1}{dz}\right)^2+\left(\frac{dP_1}{dx}\right)^2\right] \end{aligned} \tag{5}$$

where α_{ijk}^{fm} are the misfit modified (or renormalized) free energy coefficients [59]. We do not consider any strain relaxation in these structures as this would overly complicate the analyses of the results that are already not so straightforward to interpret as we shall present in the following sections. The potential in Eq. (5) has to be

minimized according to

$$\frac{dF_{FE}}{dP_i} - \sum_i \frac{d}{dx_i}\left(\frac{dF_{FE}}{dg_i}\right) = 0 \tag{6}$$

with $g_i = dP_i/dx_i$ (i = 1,2,3). The problem can be reduced to two dimensions keeping in mind that these systems typically form stripe domains along at least one of the dimensions [54,60], meaning a cross-section through the stack exposing one of the (100) or (010) planes with (001) being the base plane along the interface will be sufficient to study the properties of gPSTs. Doing so and applying the procedure in Eq. (6) for a given layer yields Euler-Lagrange equations of state for each layer as:

$$2\alpha_3^{fm}P_3 + 4\alpha_{13}^{fm}P_3P_1^2 + 4\alpha_{33}^{fm}P_3^3 + 6\alpha_{111}P_3^5 + \alpha_{112}\left(4P_3P_1^4 + 8P_3^3P_1^2\right) + 2\alpha_{123}P_3P_1^4 - G\left(\frac{\partial^2 P_3}{\partial z^2} + \frac{\partial^2 P_3}{\partial x^2}\right) = E_3^f \tag{7a}$$

$$2\alpha_1^{fm}P_1 + 2\left(2\alpha_{11}^{fm} + \alpha_{12}^{fm}\right)P_1^3 + 2\alpha_{13}^{fm}P_1P_3^2 + 6\alpha_{111}P_1^5 + 2\alpha_{112}\left[3P_1^5 + 3P_1^3P_3^2 + P_1P_3^4\right] + 2\alpha_{123}P_1^3P_3^2 - G\left(\frac{\partial^2 P_1}{\partial z^2} + \frac{\partial^2 P_1}{\partial x^2}\right) = E_1^f \tag{7b}$$

that link P_i to the components of the internal electric field vector E_i (i = 1,2,3).

Using the Poisson relation $\nabla_j \cdot D_i = \rho$ (i,j = 1,2,3) which correlates the dielectric displacement vector D_i (i = 1,2,3) to the local free charge density ρ, one can then establish links between the local (scalar) electrostatic potential ϕ and the polarization gradients such that:

$$\frac{d^2\varphi^f}{dx^2} + \frac{d^2\varphi^f}{dz^2} = \frac{1}{\varepsilon_b\varepsilon_0}\left(\frac{dP_1}{dx} + \frac{dP_3}{dz} - \rho(r)\right) \tag{8a}$$

$$\rho(r) = q\left[-n^-(r) + p^+(r) + N_d^+(r)\right] \tag{8b}$$

In the above relation, q is the elementary charge, $n^-(r)$ is the free electron density, $p^+(r)$ is the hole density,$N_d^+(r)$ is the ionized donor density, ε_0 is dielectric permittivity of vacuum (in SI units), ε_b is a background dielectric constant (taken as 7 here) [61]. Each of these charge terms depend on the electronic band parameters and local electrostatic potential and are described using Fermi-Dirac distribution functions as:

$$N_D^+ = N_D\left[1 - \left(\exp\left(\frac{q(E_D - E_F - \varphi)}{kT}\right) + 1\right)^{-1}\right] \tag{9a}$$

$$n^- = N_C\left(\exp\left(\frac{q(E_C - E_F - \varphi)}{kT}\right) + 1\right)^{-1} \tag{9b}$$

$$p^+ = N_V\left[1 - \left(\exp\left(\frac{q(E_V - E_F - \varphi)}{kT}\right) + 1\right)^{-1}\right] \tag{9c}$$

where N_C is the effective density of states at the bottom of the conduction band, N_V is the effective density of states at the top of the valence band, E_C is the energy of an electron at the bottom of the conduction band, E_V is the energy of an electron at the top of the valence band, E_F is the Fermi level, and E_D is the ionization energy of the donor site that is taken with respect to the bottom of the conduction band. Note that band edges here shift only due to the internal electrostatic potential and are considered to be free from variations in the dispersion relation due to the presence of impurities (including vacancies), which, according to Tingting et al., can shrink the band gap energy by almost 0.5 eV [62,63].

The above set of relations were evaluated numerically for the gPST system with gradient schemes shown in Fig. 1b. The thermodynamic coefficients and other material parameters used in the computations are provided in Table 1. One needs to simultaneously solve Eqs. (7)–(9) with the top-bottom interface polarization boundary conditions (BCs) given as

$$\lambda\frac{\partial P_1}{\partial x} - P_1 = 0|_{z=0,h} \text{ and } \lambda\frac{\partial P_3}{\partial z} - P_3 = 0|_{z=z=0,h} \tag{10}$$

where λ is the extrapolation length determining the extent of change of polarization along the film normal at the interface and h is the total thickness of the gPST stack. h is given as the product of the number of grid points along the z-axis (thickness) n and the distance between two grid points d, taken in our computations as 0.5 nm.

The BCs for electrostatic potential are specified at the gPST-electrode interfaces as 0 V for short circuiting or $\phi = \pm V_{app}$ at top electrode (z = 100 nm, n = 200) while the bottom electrode (z = 0 nm, n = 1) is kept at zero (grounded) where V_{app} is applied voltage. Periodic BCs are employed along the plane of the structures for both the electrostatic relations and the polarization. Note that the amount of charge transfer between the FE and the electrode will depend on the Fermi level differences of the stack and the electrodes as well as direction of P_i and the internal built-in fields. As such, we resort to numerical methods to analyze the electrical and dielectric properties of gPSTs. Ideal metal electrodes are assumed for which work function is taken as that of Pt, a common electrode material with which the Fermi level of the stack is equilibrated. The charges due to the spontaneous polarization of the FE layer at the gPST-electrode interfaces are assumed to be completely screened. The average of amplitude of the out-of-plane polarization $<|P_3|>$ is saved after each run for a given T and position in the computational grid such that

Table 1
Material parameters and thermodynamic coefficients for PT, ST, and PST used in the calculations (compiled from Ref. [79] and Ref. [59]).

	$PbTiO_3$	$SrTiO_3$
Lattice parameter (nm)	0.3935	0.3904
T_C (°C)	492	−253
C (10^5 °C)	1.5	0.8
Q_{11} (m^4/C^2)	0.089	0.0457
Q_{12} (m^4/C^2)	−0.026	−0.013
Q_{44} (m^4/C^2)	0.0675	0.00957
s_{11} (10^{-12} N/m^2)	8.0	3.729
s_{12} (10^{-12} N/m^2)	−2.5	−0.9088
S_{44} (10^{-12} N/m^2)	9	9.2
α_{11} (10^7 N m^6/C^4)	−7.253	170
α_{12} (10^8 N m^6/C^4)	7.5	27.4
α_{111} (10^8 N m^{10}/C^6)	2.606	–
α_{112} (10^8 N m^{10}/C^6)	6.1	–
α_{123} (10^9 N m^{10}/C^6)	−3.66	–
g (10^{-10} J m^3/C^2)	5	5
N_V, N_C (m^{-3})	10^{24}, 10^{24}	10^{24}, 10^{24}
E_V, E_C, E_D (eV)	−6.72, −4.0, −4.1	−7.1, −3.9, −4.0

$$<|P_3|> = \frac{\sum_N |P_3(r)|}{N} \quad (11)$$

where $N = 200 \cdot n$ is the total number of sites. Such a resolution allows us unambiguously determine the transition temperature since the transition from a PE to a FE MD state will amount to a zero change of average polarization. The dielectric response of the gPST stacks at or far from T_C is computed via

$$\varepsilon_r^{gFE} = \frac{(100 \times 10^{-9})\left[D_3^{Top}@V_{App} + 0.001 - D_3^{Top}@V_{App}\right]}{\varepsilon_0 \times 0.001} \quad (12)$$

at the end of 5000 iterations for a given T. Here 1 mV (0.001 V in Eq. (12) in the denominator is the small signal bias and, therefore, 10^4 V/m is the small signal electric field we use to probe the dielectric response of a 100 nm thick film, D_3^{Top} is the average dielectric displacement at the top gPST/electrode interface given by $\varepsilon_0\varepsilon_b E_3^{Top} + P_3^{Top}$ with superscript "*Top*" indicating the very top row of the computational grid that is in contact with the top electrode. Eq. (12) contains V_{App} that, when non-zero, allows us to compute the dielectric response under bias. We employ a finite difference discretization and carry out a Gauss-Seidel iterative scheme to solve the coupled Eqs. (1), (4), (5), (11), (12) simultaneously subject to BCs discussed above. The computation grid consists of $N = 200 \cdot n = 40{,}000$ points for all gPST stacks corresponding to a total film thickness of 100 nm. We terminate the solution after 5000 iterations that yield a difference of about 10^{-5} C/m^2 for P_1 and P_3 between two consecutive steps.

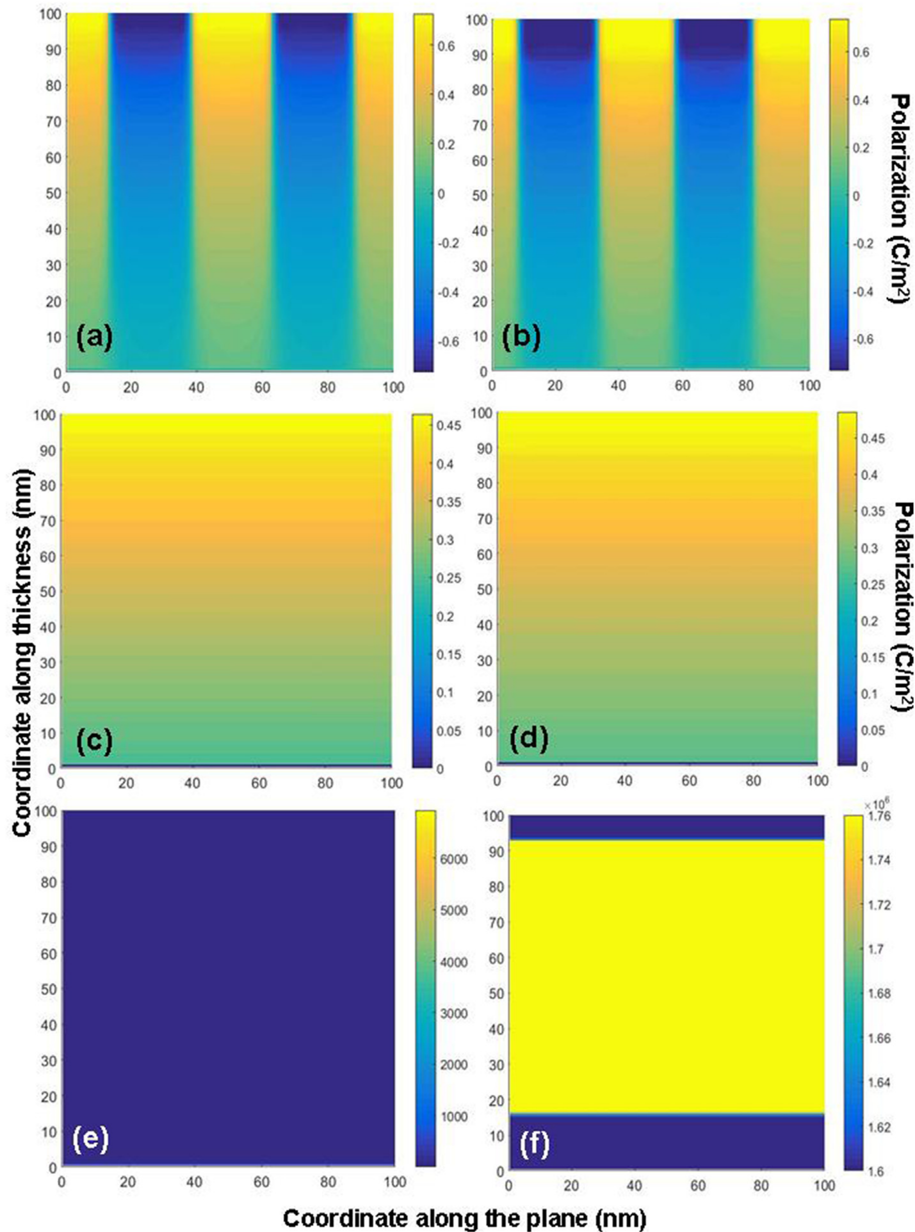

Fig. 2. Polarization map of gPST with **(a)** smooth gradient and **(b)** with coarse gradient, both being intrinsic (no impurities), and **(c)** smoothand **(d)** with coarse stacks, both with 10^{25} m^{-3} donor type impurity densities. In **(e)**, the free electron density map (m^{-3}) of gPST with coarse layers with 10^{25} m^{-3} donor type impurity density is plotted and **(f)** is the space charge distribution that only consists of ionized donors (C m^{-3}) for the gPST heterostructure in (e). No electrical domains are observed for the cases with impurities and single domain state appears to have set in at RT.

3. Room temperature domain structures

We first provide in Fig. 2 the electrical domain structures obtained by solving Eqs. (1), (4), (5), (11), (12) for the stack treated as an intrinsic semiconductor and the stack with ionizable donor impurities. Fig. 2a and b shows that the gPSTs, regardless of the layer thickness, split into electrical domains at RT. The domain periods in both stacks are identical but there is a transition from rectangular domains (top layers) to a sinusoidal pattern as the local T_C of layers is reduced (bottom layers) with increasing Sr concentration (Fig. 3). We observe the same type of behavior for low-to-moderate impurity densities (10^{23} to 10^{24} m^{-3}) but exceeding 10^{24} m^{-3}, we notice that a single-domain (SD) state is stabilized in the stacks, again regardless of the layer thicknesses. Fig. 2c and d shows that a SD structure is formed for an ionizable donor density of 10^{25} m^{-3}, a value close to previously reported experimental charge densities in 150–400 nm thick PZT films with depletion near the electrodes [58].

It is crucial to understand if this outcome is a result of possible free carriers that could compensate the internal depolarizing fields due to periodic jumps in P_3 from layer to layer. To do so, we mapped the charge distributions in the stacks and found out that both of the stacks are actually almost completely depleted of free carriers and that it is the internal electric field generated by ionized, fixed donors that is responsible for the SD state. This is shown in Fig. 2e and f where we provide free electron density maps of the two graded structures for donor type impurity density of 10^{25} m^{-3} and the space charge distribution that only consists of ionized donors, respectively. This is a very different mechanism compared to monolayer films in which electrical domains are shown to retain their presence for high space charge densities as demonstrated previously [64,65] and later on confirmed by Cheah et al. [66] It must be noted here that the space charges are only due to fixed ionized donors and this is what induces the SD state.

We can determine the electric field in the center of the coarsely and smoothly graded stacks from the gradients of the electrostatic potential found from Eq. (8a). The variation of the electric field in these heterostructures is shown in Fig. 4a and b for smooth and coarse gradients with and without (intrinsic) donors. Note that, for the intrinsic gPST, we provide the fields in only "up" domains and the "down" domains have a similar magnitude but opposite sign.

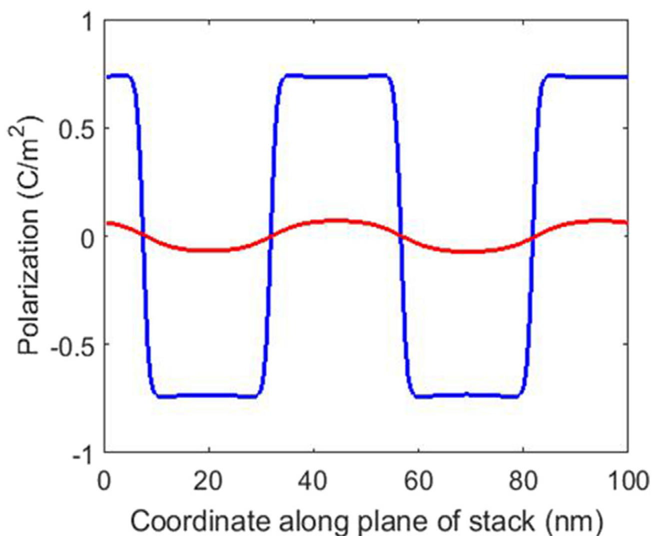

Fig. 3. The polarization amplitudes at the high T_C and the low T_C layers in the coarse graded stack. The rectangular domain shape changes to a sinusoidal morphology with variation in the composition from high T_C (PT layer) to low T_C (PST with $f = 0.7$).

We observe that ionized donors generate significantly large internal electric fields around or exceeding 10^8 V/m compared to intrinsic gPST which is in MD state. In this state, the internal fields are reduced due to electrical domains that form to minimize the gradient in P_3. The electric fields within the intrinsic stacks change along the thickness of the heterostructure in a step-wise fashion and are oscillatory: this is the result of the complications induced due to periodic variations in P_3 within the domains near each interface and is more pronounced in the stack with a coarse grading scheme. The smoothly graded gPST has a more homogeneous distribution (less oscillatory fields) as gradients in P_3 are less favorable for a varying composition over shorter distances. Such differences produce noticeable but still not very different phase transformation characteristics which can be understood from the evolution of P_3 with T and the temperature dependence of the dielectric response.

4. Phase transition characteristics

We first compare $<|P_3|>$ obtained from Eq. (6) as a function of T for coarsely and smoothly gPSTs in Fig. 5. The results are provided for both intrinsic gPST and for gPST with impurities (Fig. 5a and b, respectively). As one might anticipate, heterostructures for which

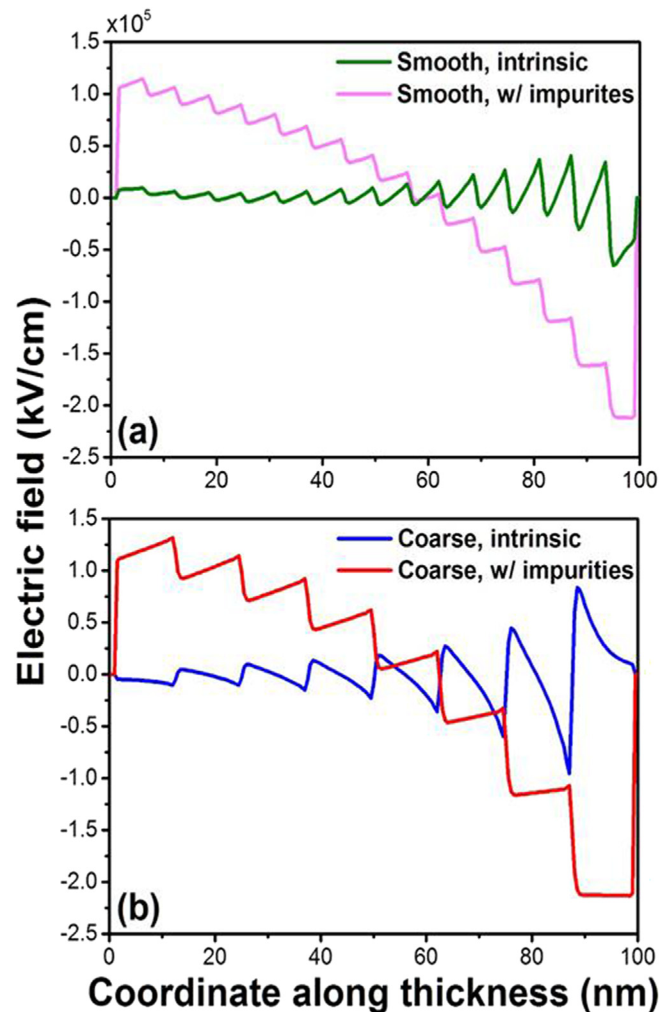

Fig. 4. Internal electric fields along the heterostructure thickness in **(a)** smoothly gPST with impurities (pink) and intrinsic gPST (green) and **(b)** coarsely gPST with impurities (red) and intrinsic gPST (blue). (For interpretation of the references to colour in this figure legend, the reader is referred to the web version of this article.)

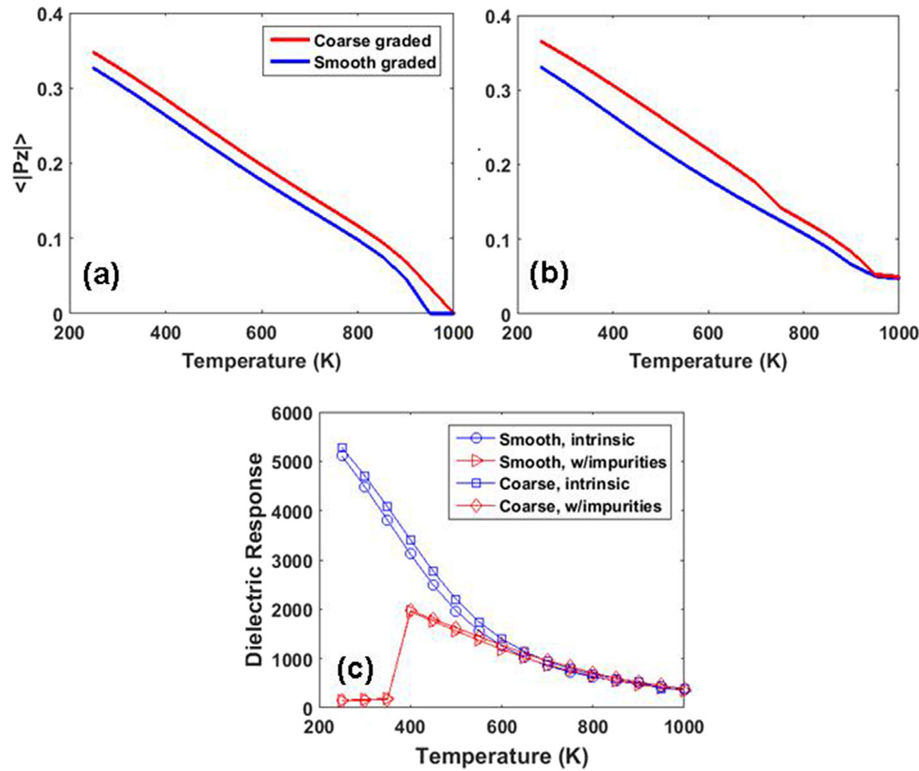

Fig. 5. The average along the film thickness polarization $<|P_3|>$ as a function of temperature for **(a)** the intrinsic gPST and **(b)** gPST heterostructure with 10^{25} m^{-3} donor impurities. Note that a built-in polarization exists in (b) and its magnitude is independent of the total layer thickness. **(c)** Dielectric response as a function of temperature for smooth and coarse gPST for the intrinsic state and with donor impurities.

the composition changes at shorter distances across the thickness leads to a slight but visible reduction in the average out-of-plane polarization $<|P_3|>$ as well as T_C. gPSTs with impurities show an identical behavior with the exception that both coarsely and smoothly graded stacks undergo a FE-to-PE transition around the same T (~950 K) and there is a strong built-in through-thickness polarization as evident from the flat part of the non-zero polarization curves above 950 K (see Fig. 4b) which is essentially the *effective* T_C of the intrinsic *and* doped gPST (Fig. 4a and b).

In all four cases of gPST, the amplitude of P_3 ($<|P_3|>$) evolves in an almost linearly decaying fashion. This is quite different than that of a strained monolayer FE film which displays a characteristic 2nd order phase transition due to the clamping effect of the substrate [59]. Despite the significant effects the presence of ionized impurities generate in the graded stacks at RT (including the stabilization of a SD state), the apparent phase transformation behavior as described by the $<|P_3|>$ - T curves are almost identical for the intrinsic stacks and the stacks with impurities (Fig. 4). The slope changes in $<|P_3|>$ curves in the gPSTs in Fig. 4b is related to stabilization of an in-plane polarization P_1 around 700 K. We note that P_1 is not as sensitive as P_3 to internal fields since the conjugate electric field E_1 in Eq. (7) is significantly weaker than E_3 and P_1 is indirectly coupled to P_3.

Such consequences do not directly imply differences in 2nd order derivatives of the energy of the gPSTs such as the dielectric response. Plotting the small-signal (relative) dielectric response for the coarsely and smoothly layered gPST in Fig. 5c, we find that the grading scheme (i.e., the relative thickness of the individual layers that make up the graded stack) does not have a substantial impact on the response of the intrinsic gPSTs. Moreover, both coarse and smooth stacks do not exhibit any sign of a dielectric anomaly at their relevant T_C regardless of their intrinsic or extrinsic (with ionizable impurities) nature. The dielectric permittivity decreases continuously with increasing T when T^1 RT as reported in experimental studies for a number of systems with composition grading [8,53]. It is seen from Fig. 5c that the dielectric response of extrinsic gPST heterostructures, i. e., those with ionizable donor impurities, are different when T À 600 K. The MD state is always stable in the intrinsic gPSTs and have a smooth evolution of the dielectric response. The dielectric permittivity is reduced for both coarse and smooth extrinsic gPST and exhibit a step around 380 K, which we find, is due to a SD-like-to-MD transition during heating. We call this as “SD-like,” since different layers have different tendencies, noting that the domain structure and the amplitude of P_3 can vary from layer to layer. It was already shown in Fig. 2 that the SD state near RT is stable (in the presence of ionizable impurities) but as the temperature is raised, the MD state replaces the SD, noticeable from the jump in the dielectric response around 380 K. The SD dielectric response comes from an incremental change in an almost unidirectional D_3 under a small signal bias while the MD dielectric response contains domain wall motion that produces a relatively big change in D_3. This explains the variation in the dielectric response when the SD-to-MD transition occurs. On the other hand, presence of space charge due to ionized impurities appear to have a negligible sensitivity to whether the grading is smooth or coarse as the two dielectric curves almost overlap (Fig. 5c). Such an outcome can also be understood keeping in mind that the electric fields across the two extrinsic stacks have identical behavior with almost identical amplitudes, albeit smaller jumps in the smooth graded gPST. At elevated T, the curves of the intrinsic and extrinsic stacks tend to merge towards a single curve, a consequence of the thermal effects that become dominant especially in the intrinsic stacks and that free carrier densities and total charge density in both stacks become identical leading to identical

dielectric response. This is also a well-known phenomena in semiconductors when the ionization energy of dopants is well below kT.

5. Band bending effects: A semi-qualitative explanation of low loss behavior in graded stacks

We finally discuss the band bending that is expected to occur within the stacks due to the variations in P_3 across the layers generating local electrical potential gradients. In Fig. 6 we provide the flat band energy diagrams for the intrinsic stacks. Such plots are obtained by superimposing the computed electrostatic potential over the flat band edge energies of the layers at zero potential drop, same as that of flat band energy diagrams of semiconductor junctions. In Fig. 6, one can see that the highest potential drop occurs in the layer with the highest T_C. This is due to the fact that largest jump in the polarization is expected to occur between this layer and the next one, resulting in a significant band bending. Moreover, as the intrinsic stacks split into electrical domains, the band bending alternates from domain to domain due to the direction of P_3 in each domain that extend through the stack thickness. As we penetrate further into the stack towards the low T_C layers, variations in P_3 get damped out and the stack tends towards a more homogeneous flat-band structure with a subsequent transition into a sinusoidal domain state as shown in Fig. 2 concurrent with a reduction in amplitude of P_3. This effectively diminishes polarization bound charge effects, hence the depolarizing fields. Notably, the stack with thin layers (smooth gradient) "feels" the band bending to a lesser extent as the polarization gradients are not favored at shorter distances within which the T_C changes due to composition variations (Fig. 6). These discussions hold for the intrinsic stacks (no space charges hence extrinsic effects) and, keeping in mind that such structures often have impurities, it remains important to address, at least qualitatively, experimental observations on low dielectric loss in such structures.

We provide next the same plots but this time for gPSTs with 10^{25} m^{-3} donor impurities in Fig. 7. It is clear that the energy band variation is quite different than the intrinsic stacks shown in Fig. 6. This is related to the electrical potential profile generated by an almost homogeneous density of ionized donors distributed along the thickness of the graded heterostructure. Superimposing the electrostatic potential onto the band edge energies provided in Table 1, we compute the band bending in each layer. The bending of the bands is quite remarkable as shown in Fig. 7 for both coarsely and smoothly gPST. Maximum band bending occurs near the middle of the heterostructures. This implies that free electrons are to be expected to accumulate near the interfaces. The midsection of the stack will act as an electrostatic potential barrier that needs to be overcome for charge transport for carriers originating from the gPST-electrode interfaces.

Furthermore, the gPSTs with donor impurities are in almost fully depleted state. This is illustrated in Fig. 8a and b which plot free electron density maps at RT under zero bias for monolayer PT and gPST, respectively. In both maps, we use the same impurity density corresponding to 10^{25} m^{-3}. That the extrinsic gPST stacks are fully depleted is entirely consistent with reports showing low tangent losses (with respect to extrinsic monolayer films) even at low frequencies (<10 kHz) where conductivity losses dominate in dielectrics, implying a small imaginary part of the dielectric response due to low free carrier densities [8,52,53,67]. Our results here semi-qualitatively reveal the mechanism behind this difference between the gPSTs and monolayer FEs. Overall, it is quite

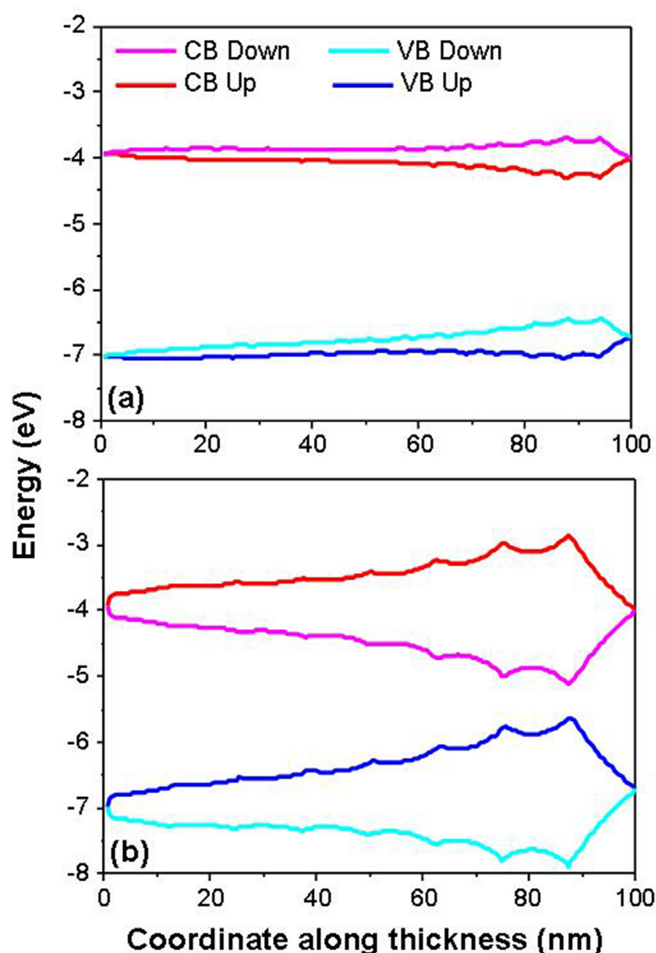

Fig. 6. Room temperature flat band energy diagrams for intrinsic **(a)** smooth and **(b)** coarse gPST. Note that the bands are given for "up" and "down" domains as the potential in each domain differs. The band gap is assumed to change linearly with changing composition from PT to PST with $f = 0.7$. VB and CB in the plot correspond to the valence band top and conduction band bottom, respectively.

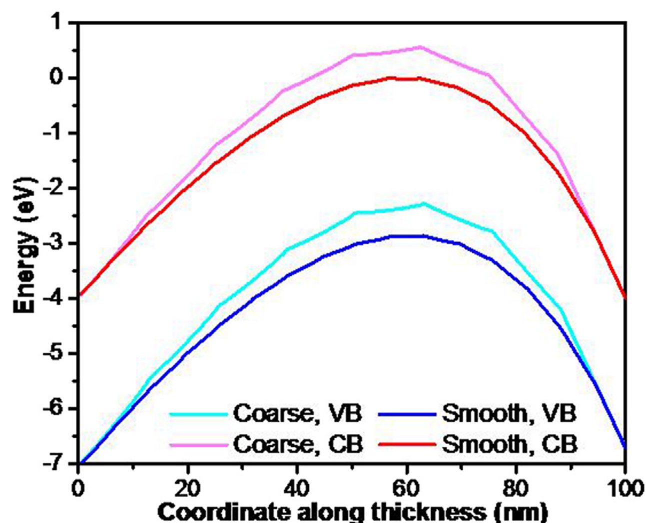

Fig. 7. Room temperature flat band energy diagrams for smooth and coarse gPST heterostructures. In both cases, the donor impurity density is taken to be 10^{25} m^{-3}. The band gap is assumed to change linearly with changing composition from PT to PST with $f = 0.7$. VB and CB in the plot correspond to the valence band top and conduction band bottom, respectively.

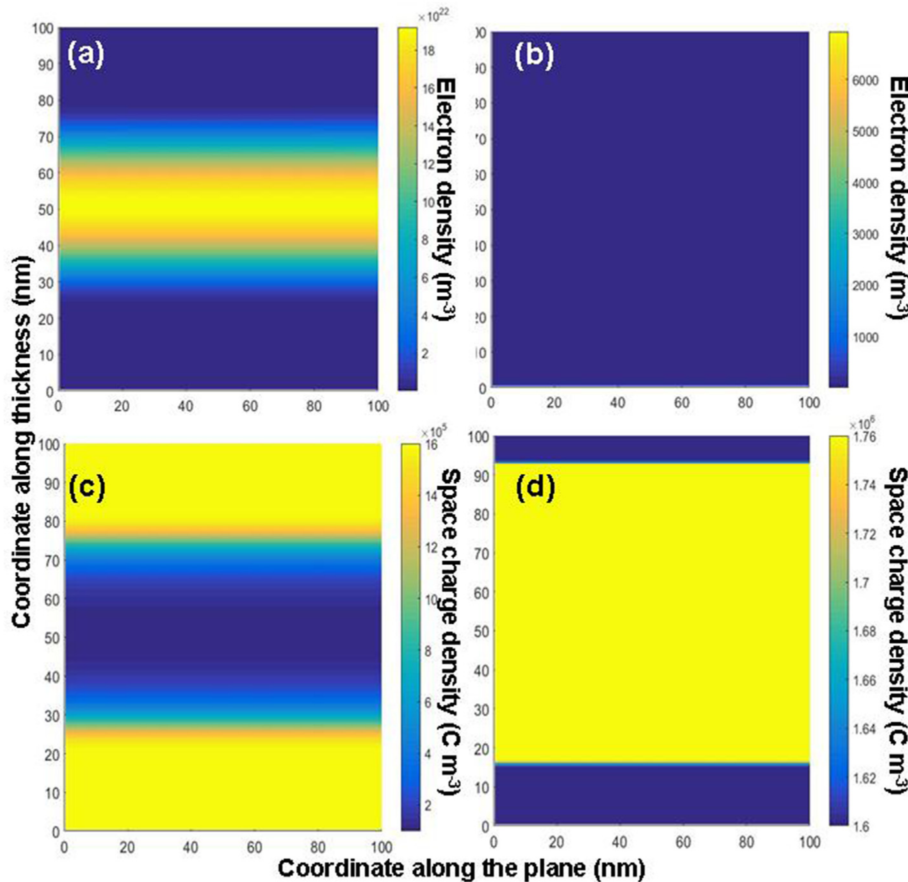

Fig. 8. Free electron density maps at room temperature under zero bias for **(a)** a monolayer PT and **(b)** coarse gPST; **(c)** and **(d)** are room temperature space charge maps in $C\cdot m^{-3}$ for donor atom densities corresponding to 10^{25} m^{-3} at zero bias for monolayer PT and coarse gPST. Notice that the graded stack in (b) is almost completely depleted despite that the electrical BCs in both (a) and (b) are the same. The difference in carrier densities between the monolayer and the graded stack is of almost 19 orders of magnitude. Both structures are in single domain state in the presence of donor impurities. gPST has almost homogeneous ionized donors density distributed within the stack, meaning that the heterostructure is depleted of free electrons. The monolayer in (c) has a clearly visible "screening length" of about 20–25 nm near top and bottom interfaces, slightly asymmetric due to P_3 pointing from bottom up, after which total charge rapidly goes to zero in the midsection where free electrons are expected to reside (hence zero space charge in this region). Holes are minority carriers and have almost zero density (not shown).

reasonable to argue that the low loss at low frequencies (10 kHz or less) reported by several groups is related to the strongly position dependent potential within the graded stacks causing a strong depletion of carriers in gPSTs. Such strongly alternating fields are also expected to give rise to Coulomb scattering for carriers flowing under an external bias, again reducing the leakage-type losses in such stacks.

6. Discussion and summary

The numerical analysis that we carried out on compositionally graded stacks in this work using a combination of thermodynamics and electrostatics reveals that there is a wide spectrum of results that can be expected in these systems. While we can identify certain trends in intrinsic stacks, where the layer thickness appears to be the only governing parameter (for a given grading scheme), presence of impurities that act similar to dopants and possible variations in top/bottom electrode properties can have a significant impact on the transition characteristics and associated anomalies. It is almost certain that such an outcome will strongly mask intrinsic material parameters including leakage currents that give rise to apparently interesting but potentially misleading interpretations of experimental observations (see e.g., Ref. [68]). Our study presented herein is a theoretical approach that takes into account electrostatic fields arising from compositional gradients and space charges. We note that in graded constructs there are a plethora of microstructural and experimental parameters that are difficult or impossible to include in a theoretical analysis. These include position dependent relaxation of in-plane strains, misfit and threading dislocations [69–73], other point/line defects, planar defects with long-range strain fields which all result in even stronger smearing of the FE transition [74]. However, we show here unambiguously that gFE stacks, regardless of presence of impurities and other lattice defects, will not exhibit a dielectric anomaly observed in bulk or monolayer films when passing through T_C upon heating/cooling. In fact, the high temperature behavior of the dielectric response appears to be almost independent of the defect content, layer thicknesses, and the electrical boundary conditions for a given grading scheme. A similar result was also reported previously for Pb(Zr,Ti)O_3/$SrTiO_3$ superlattices [56]. Such superlattices, despite the varying period and the repeating unit type, were found to be insensitive to variations in dielectric response at temperatures higher than 700 K. Results obtained for superlattices appear to be more straightforward to interpret as these structures can even be evaluated considering one repeating unit as shown in another earlier study [55]. Compositionally graded structures, however, need to be taken as a whole as there is no repeating unit, making the properties and T_C of the graded stacks a function of total thickness, unlike the superlattices in the ideal electrode limit. Therefore, total thickness of the graded stacks becomes an important design parameter as

well.

Another important result we demonstrate theoretically is that free carriers (such as electrons as analyzed in this study) that emanate from ionizable donors deplete the gFE constructs, leaving behind only ionized donors that appear to be the only contributor to the space charges. This assumption excludes the possibility of electron injection into the gFE from the electrodes at relatively high fields, which depends on barrier height determined by the difference between the Fermi levels of the graded stack and the electrode. The important SC parameters that would impact the carrier concentrations (hence the dielectric loss) and their distribution in this study are the effective density of states near the band edge energies, impurity concentrations, and the difference between the Fermi levels of the gFE and the electrode metal (see Ref. [75] for a demonstrative analysis for $Pb(Zr,Ti)O_3$ films synthesized with different electrodes). Effective density of states in $BaTiO_3$ as high as 10^{25} m^{-3} were reported (an order of magnitude higher than what is used in this study) and used in calculations [76] but here this is not of significance as we limit the impurity concentration to similar values, keeping the Fermi level of the gFE within the band gap. For results significantly more different than what is reported here, there should be significant variations in the effective density of states and band edge energies as well as the work functions of the electrodes. For instance, an electrode with a work function close to that of the electron affinity of an *n*-type gFE could, in principle, allow carrier presence within the stack albeit dependence on polarization gradients. The presence of ferroelectric polarization comes in as another additional parameter that contributes to the band bending throughout the gFE thickness via the internal electrostatic potential variation it generates due to its spatial variance from layer to layer. In monolayer films, for example, the direction of polarization (when along the normal of the plane of the film) is, in fact, so important that it can change the electronic character of an interface (Ohmic or Schottky type) [77,78] as the band edges can “almost dip” into or “float away” from the Fermi level of the system near the interfaces where the polarization terminates either with a negative or positive sign. For commonly used electrode materials, such as noble metals (Pt, Au, Pd, and similar) or conducting oxides ($SrRuO_3$ and similar) having work functions ϕ_M of ~ 5–5.5 eV, our results are valid as Schottky-type interfaces are expected for $\phi_M > E_F$ for *n*-type impurities. Here, E_F is the Fermi level of the FE/ferroic material. That carriers deplete the graded stacks due to large internal built-in fields is a possible explanation for low losses often reported in these structures. This is in addition to the periodic variation in the electrostatic potential along the thickness that can act as a barrier if leakage currents if charge injection from electrodes develop. Repeating the same calculation but for a monolayer PT reveals that partial depletion is expected in monolithic films of almost the same thickness and impurity density. Under such circumstances, we expect significantly higher losses compared to compositionally graded FEs.

In summary, we must emphasize that there is a very wide spectrum of electronic, electrical, and dielectric properties that can be expected from FE multilayers and compositionally graded heterostructures. A clear consequence here is that it is prohibitively difficult to devise a straightforward approach to correlate the dielectric response to a particular set of interrelated material parameters and boundary conditions such as layer thickness, top/bottom electrode asymmetry, and extrinsic effects. While inherent complexities related to electrostatic interactions in graded ferroelectrics make it difficult for intuitive experimental approaches in design of such systems with desired functionalities, these materials are ideally suited for systematic materials-by-design concepts guided by multi-scale theoretical methods.

Acknowledgements

The authors gratefully acknowledge many useful discussions with J. V. Mantese (United Technologies Research Center). They also would like thank M. T. Kesim (UConn) for his help with the figures.

References

[1] A. Neubrand, J. Rodel, Gradient materials: an overview of a novel concept, Z. Fur Met. 88 (1997) 358–371.
[2] D.C. Pender, N.P. Padture, A.E. Giannakopoulos, S. Suresh, Gradients in elastic modulus for improved contact-damage resistance. Part I: the silicon nitride-oxynitride glass system, Acta Mater. 49 (2001) 3255–3262.
[3] W.Y. Lee, D.P. Stinton, C.C. Berndt, F. Erdogan, Y.D. Lee, Z. Mutasim, Concept of functionally graded materials for advanced thermal barrier coating applications, J. Am. Ceram. Soc. 79 (1996) 3003–3012.
[4] M. Brazier, M. McElfresh, S. Mansour, Unconventional hysteresis behavior in compositionally graded Pb(Zr,Ti)O-3 thin films, Appl. Phys. Lett. 72 (1998), 1121-+.
[5] D.H. Bao, N. Mizutani, X. Yao, L.Y. Zhang, Structural, dielectric, and ferroelectric properties of compositionally graded (Pb,La)TiO3 thin films with conductive LaNiO3 bottom electrodes, Appl. Phys. Lett. 77 (2000) 1041–1043.
[6] J.V. Mantese, N.W. Schubring, A.L. Micheli, Polarization-graded ferroelectrics: transpacitor energy gain, Appl. Phys. Lett. 79 (2001) 4007–4009.
[7] J.V. Mantese, N.W. Schubring, A.L. Micheli, Polarization-graded ferroelectrics: transpacitor push-pull amplifier, Appl. Phys. Lett. 80 (2002) 1430–1431.
[8] X.H. Zhu, J.M. Zhu, S.H. Zhou, Z.G. Liu, N.B. Ming, H.L.W. Chan, C.L. Choy, K.H. Wong, D. Hesse, Microstructure and dielectric properties of compositionally-graded (Ba1-xSrx)TiO3 thin films, Mater. Sci. Eng. B-Solid State Mater. Adv. Technol. 118 (2005) 219–224.
[9] H.X. Cao, V.C. Lo, Z.Y. Li, Dielectric response of temperature-graded ferroelectric films, J. Appl. Phys. 98 (2005) 114105.
[10] S. Zhong, Z.G. Ban, S.P. Alpay, J.V. Mantese, Large piezoelectric strains from polarization graded ferroelectrics, Appl. Phys. Lett. 89 (2006) 142913.
[11] J.W. Zhai, C. Gao, X.K. Yao, Z.K. Xu, H.D. Chen, The tunability and dielectric properties of the compositionally graded Ba(ZrxTi1-x)O-3 thin films, J. Electroceramics 21 (2008) 12–16.
[12] D. Wu, H. Wu, Z. Fu, C. Zhao, A.D. Li, Polarization offsets of compositionally graded Nd-substituted Bi(4)Ti(3)O(12) ferroelectric thin films, Appl. Phys. Lett. 93 (2008) 062904.
[13] C. Bhardwaj, B.S.S. Daniel, D. Kaur, Highly tunable compositionally graded (1-x)Ba(Zr0.2Ti0.8)O-3-x(Ba0.7Ca0.3)TiO3 multilayer with low temperature capacitance coefficients, Mater. Lett. 87 (2012) 172–175.
[14] R.V.K. Mangalam, J.C. Agar, A.R. Damodaran, J. Karthik, L.W. Martin, Improved pyroelectric figures of merit in compositionally graded PbZr1-x,TixO3 thin films, Acs Appl. Mater. Interfaces 5 (2013) 13235–13241.
[15] L.W. Zhang, X.H. Hao, J.C. Yang, S.L. An, B. Song, Large enhancement of energy-storage properties of compositional graded (Pb1-xLax)(Zr0.65Ti0.35)O-3 relaxor ferroelectric thick films, Appl. Phys. Lett. 103 (2013) 113902.
[16] R.V.K. Mangalam, J. Karthik, A.R. Damodaran, J.C. Agar, L.W. Martin, Unexpected crystal and domain structures and properties in compositionally graded PbZr1-xTixO3 thin films, Adv. Mater. 25 (2013) 1761–1767.
[17] Z.Q. Gu, M.A. Islam, J.E. Spanier, Giant enhancement in the ferroelectric field effect using a polarization gradient, Appl. Phys. Lett. 107 (2015) 162901.
[18] H. Morkoc, R. Cingolani, B. Gil, Polarization effects in nitride semiconductor device structures and performance of modulation doped field effect transistors, Solid-State Electron. 43 (1999) 1909–1927.
[19] M.A. Khan, J.W. Yang, G. Simin, R. Gaska, M.S. Shur, A.D. Bykhovski, Piezoelectric doping in AlInGaN/GaN heterostructures, Appl. Phys. Lett. 75 (1999) 2806–2808.
[20] O. Ambacher, B. Foutz, J. Smart, J.R. Shealy, N.G. Weimann, K. Chu, M. Murphy, A.J. Sierakowski, W.J. Schaff, L.F. Eastman, R. Dimitrov, A. Mitchell, M. Stutzmann, Two dimensional electron gases induced by spontaneous and piezoelectric polarization in undoped and doped AlGaN/GaN heterostructures, J. Appl. Phys. 87 (2000) 334–344.
[21] G. Martinez-Criado, A. Cros, A. Cantarero, O. Ambacher, C.R. Miskys, R. Dimitrov, M. Stutzmann, J. Smart, J.R. Shealy, Residual strain effects on the two-dimensional electron gas concentration of AlGaN/GaN heterostructures, J. Appl. Phys. 90 (2001) 4735–4740.
[22] H.K. Chan, C.H. Lam, F.G. Shin, Time-dependent space-charge-limited conduction as a possible origin of the polarization offsets observed in compositionally graded ferroelectric films, J. Appl. Phys. 95 (2004) 2665–2671.
[23] G. Akcay, S. Zhong, B.S. Allimi, S.P. Alpay, J.V. Mantese, Strain induced internal potentials of compositionally graded epitaxial ferroelectric thin films, Appl. Phys. Lett. 91 (2007) 012904.
[24] J. Karthik, R.V.K. Mangalam, J.C. Agar, L.W. Martin, Large built-in electric fields due to flexoelectricity in compositionally graded ferroelectric thin films, Phys. Rev. B 87 (2013) 024111.
[25] Y. Zhao, X.H. Hao, Q. Zhang, Enhanced energy-storage performance and electrocaloric effect in compositionally graded Pb(1-3x/2)LaxZr0.85Ti0.15O3 antiferroelectric thick films, Ceram. Int. 42 (2016) 1679–1687.
[26] M.B. Okatan, J.V. Mantese, S.P. Alpay, Effect of space charge on the polarization

hysteresis characteristics of monolithic and compositionally graded ferroelectrics, Acta Mater. 58 (2010) 39–48.
[27] F. Xue, J.J. Wang, G. Sheng, E. Huang, Y. Cao, H.H. Huang, P. Munroe, R. Mahjoub, Y.L. Li, V. Nagarajan, L.Q. Chen, Phase field simulations of ferroelectrics domain structures in PbZrxTi1-xO3 bilayers, Acta Mater. 61 (2013) 2909–2918.
[28] V.M. Fridkin, Ferroelectric Semiconductors, first ed., Consultants Bureau, 1980.
[29] S. Piskunov, E. Heifets, R.I. Eglitis, G. Borstel, Bulk properties and electronic structure of SrTiO3, BaTiO3, PbTiO3 perovskites: an ab initio HF/DFT study, Comput. Mater. Sci. 29 (2004) 165–178.
[30] F. Jin, G.W. Auner, R. Naik, N.W. Schubring, J.V. Mantese, A.B. Catalan, A.L. Micheli, Giant effective pyroelectric coefficients from graded ferroelectric devices, Appl. Phys. Lett. 73 (1998) 2838–2840.
[31] S.G. Lu, X.H. Zhu, C.L. Mak, K.H. Wong, H.L.W. Chan, C.L. Choy, High tunability in compositionally graded epitaxial barium strontium titanate thin films by pulsed-laser deposition, Appl. Phys. Lett. 82 (2003) 2877–2879.
[32] Z.G. Ban, S.P. Alpay, J.V. Mantese, Fundamentals of graded ferroic materials and devices, Phys. Rev. B 67 (2003) 184104.
[33] L. Pintilie, I. Boerasu, M.J.M. Gomes, Simple model of polarization offset of graded ferroelectric structures, J. Appl. Phys. 93 (2003) 9961–9967.
[34] C.K. Wong, F.G. Shin, Modeling of anomalous hysteresis behavior of compositionally graded ferroelectric films at low fields, J. Appl. Phys. 98 (2005) 024104.
[35] M.Y. El-Naggar, K. Dayal, D.G. Goodwin, K. Bhattacharya, Graded ferroelectric capacitors with robust temperature characteristics, J. Appl. Phys. 100 (2006) 114115.
[36] J.W. Zhai, X. Yao, Z.K. Xu, H. Chen, Ferroelectric properties of PbxSr1-xTiO3 and its compositionally graded thin films grown on the highly oriented LaNiO3 buffered Pt/Ti/SiO2/Si substrates, J. Appl. Phys. 100 (2006) 034108.
[37] A.L. Roytburd, J. Slutsker, Thermodynamics of polydomain ferroelectric bilayers and graded multilayers, Appl. Phys. Lett. 89 (2006) 042907.
[38] H.Y. Zhang, Z.Y. Zhu, X.H. Zhang, J.C. Han, Polarization and dielectric properties of ferroelectric thin film grown compositionally graded substrate: the first-principles study, Solid State Commun. 144 (2007) 339–342.
[39] A. Khodorov, S.A.S. Rodrigues, M. Pereira, M.J.M. Gomes, Dielectric nonlinearity in a compositionally graded lead zirconate titanate structure, J. Appl. Phys. 104 (2008) 126102.
[40] M.B. Okatan, M.W. Cole, S.P. Alpay, Dielectric tunability of graded barium strontium titanate multilayers: effect of thermal strains, J. Appl. Phys. 104 (2008) 104107.
[41] M.B. Okatan, A.L. Roytburd, J.V. Mantese, S.P. Alpay, Domain engineering in compositionally graded ferroelectric films for enhanced dielectric response and tunability, J. Appl. Phys. 105 (2009) 114106.
[42] A.L. Roytburd, V. Roytburd, J. Slutsker, Domain structures in continuously graded ferroelectric films, Appl. Phys. Lett. 94 (2009) 152904.
[43] A. Roytburd, V. Roytburd, Domain evolution and polarization of continuously graded ferroelectric films, Philos. Mag. 90 (2010) 61–69.
[44] V.N. Shut, S.R. Syrtsov, V.L. Trublovsky, Polarization characteristics of graded thick Ba1-xSrxTiO3 films, Phys. Solid State 53 (2011) 1859–1866.
[45] M.B. Okatan, A.L. Roytburd, V. Nagarajan, S.P. Alpay, Electrical domain morphologies in compositionally graded ferroelectric films, J. Phys. Condens. Matter 24 (2012) 024215.
[46] V.N. Shut, Ferroelectrics with composition gradient: on the nature of hysteresis loop shift, Phys. Solid State 55 (2013) 1438–1441.
[47] J.C. Agar, A.R. Damodaran, G.A. Velarde, S. Pandya, R.V.K. Mangalam, L.W. Martin, Complex evolution of built-in potential in compositionally-graded PbZr1-xTixO3 thin films, ACS Nano 9 (2015) 7332–7342.
[48] J.C. Agar, A.R. Damodaran, M.B. Okatan, J. Kacher, C. Gammer, R.K. Vasudevan, S. Pandya, L.R. Dedon, R.V.K. Mangalam, G.A. Velarde, S. Jesse, N. Balke, A.M. Minor, S.V. Kalinin, L.W. Martin, Highly mobile ferroelastic domain walls in compositionally graded ferroelectric thin films, Nat. Mater. 15 (2016), 549-+.
[49] D.J. Kim, J.Y. Jo, Y.S. Kim, Y.J. Chang, J.S. Lee, J.G. Yoon, T.K. Song, T.W. Noh, Polarization relaxation induced by a depolarization field in ultrathin ferroelectric BaTiO3 capacitors, Phys. Rev. Lett. 95 (2005) 237602.
[50] J.Y. Jo, S.M. Yang, T.H. Kim, H.N. Lee, J.G. Yoon, S. Park, Y. Jo, M.H. Jung, T.W. Noh, Nonlinear dynamics of domain-wall propagation in epitaxial ferroelectric thin films, Phys. Rev. Lett. 102 (2009) 045701.
[51] S.H. Baek, H.W. Jang, C.M. Folkman, Y.L. Li, B. Winchester, J.X. Zhang, Q. He, Y.H. Chu, C.T. Nelson, M.S. Rzchowski, X.Q. Pan, R. Ramesh, L.Q. Chen, C.B. Eom, Ferroelastic switching for nanoscale non-volatile magnetoelectric devices, Nat. Mater. 9 (2010) 309–314.
[52] X.H. Zhu, N. Chong, H.L.W. Chan, C.L. Choy, K.H. Wong, Z. Liu, N. Ming, Epitaxial growth and planar dielectric properties of compositionally graded (Ba1-xSrx)TiO3 thin films prepared by pulsed-laser deposition, Appl. Phys. Lett. 80 (2002) 3376–3378.
[53] D. Maurya, F.C. Sun, S.P. Alpay, S. Priya, A new method for achieving enhanced dielectric response over a wide temperature range, Sci. Rep. 5 (2015) 15144.
[54] A.M. Bratkovsky, A.P. Levanyuk, Abrupt appearance of the domain pattern and fatigue of thin ferroelectric films, Phys. Rev. Lett. 84 (2000) 3177–3180.
[55] A.P. Levanyuk, I.B. Misirlioglu, Phase transitions in ferroelectric-paraelectric superlattices, J. Appl. Phys. 110 (2011) 114109.
[56] I.B. Misirlioglu, M.T. Kesim, S.P. Alpay, Strong dependence of dielectric properties on electrical boundary conditions and interfaces in ferroelectric superlattices, Appl. Phys. Lett. 104 (2014) 022906.
[57] M.W. Cole, E. Ngo, C. Hubbard, S.G. Hirsch, M. Ivill, W.L. Sarney, J. Zhang, S.P. Alpay, Enhanced dielectric properties from barium strontium titanate films with strontium titanate buffer layers, J. Appl. Phys. 114 (2013) 164107.
[58] L. Pintilie, I. Boerasu, M.J.M. Gomes, T. Zhao, R. Ramesh, M. Alexe, Metal-ferroelectric-metal structures with Schottky contacts. II. Analysis of the experimental current-voltage and capacitance-voltage characteristics of Pb(Zr,Ti)O-3 thin films - art. no. 123104, J. Appl. Phys. 98 (2005) 124104.
[59] N.A. Pertsev, A.G. Zembilgotov, A.K. Tagantsev, Effect of mechanical boundary conditions on phase diagrams of epitaxial ferroelectric thin films, Phys. Rev. Lett. 80 (1998) 1988–1991.
[60] A.M. Bratkovsky, A.P. Levanyuk, Continuous theory of ferroelectric states in ultrathin films with real electrodes, J. Comput. Theor. Nanosci. 6 (2009) 465–489.
[61] A.K. Tagantsev, Landau expansion for ferroelectrics: which variable to use? Ferroelectrics 375 (2008) 19–27.
[62] T.T. Qi, I. Grinberg, A.M. Rappe, Band-gap engineering via local environment in complex oxides, Phys. Rev. B 83 (2011) 224108.
[63] T.T. Qi, M.T. Curnan, S. Kim, J.W. Bennett, I. Grinberg, A.M. Rappe, First-principles study of band gap engineering via oxygen vacancy doping in perovskite ABB ' O-3 solid solutions, Phys. Rev. B 84 (2011) 245206.
[64] I.B. Misirlioglu, H.N. Cologlu, M. Yildiz, Thickness driven stabilization of saw-tooth-like domains upon phase transitions in ferroelectric thin films with depletion charges, J. Appl. Phys. 111 (2012) 064105.
[65] N. Ng, R. Ahluwalia, D.J. Srolovitz, Depletion-layer-induced size effects in ferroelectric thin films: a Ginzburg-Landau model study, Phys. Rev. B 86 (2012) 094104.
[66] W.L. Cheah, N. Ng, R. Ahluwalia, Influence of space charge on domain patterns and susceptibility in a rhombohedral ferroelectric film, Acta Mater. 100 (2015) 323–332.
[67] C.V. Weiss, M.B. Okatan, S.P. Alpay, M.W. Cole, E. Ngo, R.C. Toonen, Compositionally graded ferroelectric multilayers for frequency agile tunable devices, J. Mater. Sci. 44 (2009) 5364–5374.
[68] P. Lunkenheimer, V. Bobnar, A.V. Pronin, A.I. Ritus, A.A. Volkov, A. Loidl, Origin of apparent colossal dielectric constants, Phys. Rev. B 66 (2002) 052105.
[69] I. Vrejoiu, G. Le Rhun, N.D. Zakharov, D. Hesse, L. Pintilie, M. Alexe, Threading dislocations in epitaxial ferroelectric PbZr0.2Ti0.8O3 films and their effect on polarization backswitching, Philos. Mag. 86 (2006) 4477–4486.
[70] I.B. Misirlioglu, S.P. Alpay, M. Aindow, V. Nagarajan, Thermodynamic and electrostatic analysis of threading dislocations in epitaxial ferroelectric films, Appl. Phys. Lett. 88 (2006) 102906.
[71] M.W. Chu, I. Szafraniak, R. Scholz, C. Harnagea, D. Hesse, M. Alexe, U. Gosele, Impact of misfit dislocations on the polarization instability of epitaxial nanostructured ferroelectric perovskites, Nat. Mater. 3 (2004) 87–90.
[72] V. Nagarajan, C.L. Jia, H. Kohlstedt, R. Waser, I.B. Misirlioglu, S.P. Alpay, R. Ramesh, Misfit dislocations in nanoscale ferroelectric heterostructures, Appl. Phys. Lett. 86 (2005) 192910.
[73] I.B. Misirlioglu, A.L. Vasiliev, S.P. Alpay, M. Aindow, R. Ramesh, Defect microstructures in epitaxial PbZr0.2Ti0.8O3 films grown on (001)SrTiO3 by pulsed laser deposition, J. Mater. Sci. 41 (2006) 697–707.
[74] A.P. Levanyuk, A.S. Sigov, Defects and structural phase transitions, in: W. Taylor (Ed.), Ferroelectricity and Related Phenomena, Gordon and Breach, 1988.
[75] L. Pintilie, I. Vrejoiu, D. Hesse, M. Alexe, The influence of the top-contact metal on the ferroelectric properties of epitaxial ferroelectric Pb(Zr0.2Ti0.8)O-3 thin films, J. Appl. Phys. 104 (2008) 114101.
[76] A. Amin, Phenomenological description of stress related grain-boundary properties in semiconducting perovskites, Ferroelectrics 87 (1988) 41–53.
[77] X.H. Liu, Y. Wang, J.D. Burton, E.Y. Tsymbal, Polarization-controlled Ohmic to Schottky transition at a metal/ferroelectric interface, Phys. Rev. B 88 (2013) 165139.
[78] I.B. Misirlioglu, M. Yildiz, Carrier accumulation near electrodes in ferroelectric films due to polarization boundary conditions, J. Appl. Phys. 116 (2014) 024102.
[79] M.J. Haun, E. Furman, H.A. McKinstry, L.E. Cross, Thermodynamic theory of the lead zirconate-titanate solid-solution system, .2. PRECRITICAL behavior, Ferroelectrics 99 (1989) 27–44.